Journal of Power Sources 416 (2019) 125–131

Contents lists available at ScienceDirect

Journal of Power Sources

journal homepage: www.elsevier.com/locate/jpowsour

Understanding of pre-lithiation of poly(acrylic acid) binder: Striking the balances between the cycling performance and slurry stability for silicon-graphite composite electrodes in Li-ion batteries

Bin Hu[a,1], Sisi Jiang[a,b,1], Ilya A. Shkrob[a], Jingjing Zhang[a], Stephen E. Trask[a], Bryant J. Polzin[a], Andrew Jansen[a], Wei Chen[c,d], Chen Liao[a], Zhengcheng Zhang[a], Lu Zhang[a,*]

[a] Chemical Sciences and Engineering Division, Argonne National Laboratory, 9700 South Cass Avenue, Argonne, IL, 60439, USA
[b] Department of Chemistry, University of Tennessee, 1420 Circle Drive, Knoxville, TN, 37996, USA
[c] Institute for Molecular Engineering and Materials Science Division, Argonne National Laboratory, 9700 South Cass Avenue, Argonne, IL, 60439, USA
[d] Institute for Molecular Engineering, The University of Chicago, 5640 South Ellis Avenue, Chicago, IL, 60637, USA

HIGHLIGHTS

- Pre-lithiation treatment of PAA binder was conducted by titration with LiOH.
- The treatment affords enhanced viscosity and shear-thinning but less cohesion.
- Cycling results indicated the pre-lithiation can undermine the cell performance.
- The treatment balances the opposing trends in the cycling and slurry stability.

GRAPHICAL ABSTRACT

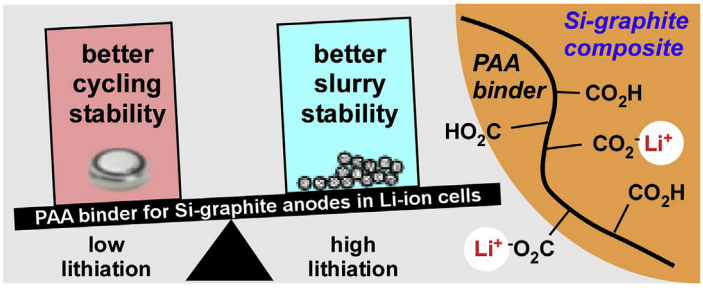

ARTICLE INFO

Keywords:
PAA binder
Silicon
Lithium-ion
Pre-lithiation
Polymer
Slurry stability

ABSTRACT

Poly(acrylic acid) (PAA) is widely used as a polymer binder for high capacity silicon (Si) anodes in Li-ion batteries. When used, the carboxyl ($-CO_2H$) groups of PAA can be partially lithiated (known as pre-lithiation treatment), which is believed to facilitates lamination process, especially for production on a large scale. However, such treatment impacts numerous physico-chemical properties of the PAA binder that affect the cycling performance of the electrode. Here we seek to quantify the pre-lithiation treatment effect on Li-ion cells containing Si-graphite composite electrodes. The electrochemical cycling results indicated that such pre-lithiation treatment of PAA can undermine the cycling performance, as more capacity loss was observed when pre-lithiated PAA binders were used. On the other hand, the same pre-lithiation practice is indeed beneficial for the lamination process, as it increases the viscosity of aqueous slurries at low shear rates (slows down sedimentation) and prompts the shear thinning (so that the slurries can be more easily mixed). Thus, there is an uneasy balance between the electrochemical performance that suffers from the pre-lithiation of PAA and the quality of slurry processing which benefits from the same practice. An alternative approach to slurry treatment would be desired to achieve better cycling performance without undermining the stability of slurry suspensions.

* Corresponding author.
E-mail address: luzhang@anl.gov (L. Zhang).
[1] Contributed equally.

https://doi.org/10.1016/j.jpowsour.2019.01.068
Received 1 October 2018; Received in revised form 22 January 2019; Accepted 23 January 2019
0378-7753/

1. Introduction

Graphite (Gr), which is commonly used as electrode material for lithium-ion batteries (LIBs), has relatively low gravimetric (372 mAh g^{-1}) and volumetric (890 mAh cm^{-3}) capacity, and these limitations circumscribe possible improvements of LIBs using this material [1]. Among the alternative materials, silicon (Si) stands out due to its low cost and high theoretical capacity (~4200 mAh g^{-1} gravimetric capacity based on the $Li_{4.4}Si$ alloy and volumetric capacity of ~9800 mAh cm^{-3} based on initial volume) [2–4]. However, large volumetric changes in Si particles during Li alloying (~320 vol%) cause their fracture and electric isolation of silicon cores, while continuous formation and breaking down of protective solid-electrolyte interphase (SEI) formed on these unstable particles causes capacity fade [4–7]. Given these tendencies, stiff polymer binders that provide strong cohesion between particles in the electrode matrix and offer resistance to volumetric changes in the Si particles can significantly improve the cycling performance of Si-based anodes [8,9]. The conventional polymer binder used in graphite electrodes, poly(vinylidene fluoride) (PVdF), is not suitable for such Si-based anodes due to its low tensile strength and poor adhesion to Si surface. Water soluble polymers with hydroxyl or carboxylate groups, such as alginate, carboxymethyl cellulose (CMC) and poly(acrylic acid) (PAA) show greater promise, as their functional groups may help to form strong covalent bonds with siloxyl (SiOH) groups on the Si surface maintaining cohesion during volumetric changes [10–13].

Among these materials, PAA based binders are particularly attractive due to a combination of excellent performance in the electrodes and low cost [12,14,15]. The protons in the $-CO_2H$ (carboxylate) groups of PAA can be partially exchanged by Li^+ ions (this is known as pre-lithiation treatment), which is a common practice for fabrication of Si-containing anodes. Such "pre-lithiated PAA" (that is, PAA titrated with LiOH to pH ~7) has become the standard binder material for Silicon Deep Dive program that is funded by DOE [16,17]. While PAA binder is becoming increasingly used, the factors controlling its performance in the LIBs are not fully understood [18]. In particular, it is believed that the pre-lithiation treatment benefits the lamination process (especially for a large scale production) by yielding mechanically cohesive and uniform electrodes at relatively high loadings of active materials [19]. However, very few study has been conducted to look into the mechanism behind. Moreover, this practice involves the strong base, LiOH, which can considerably increase the pH of the slurries, changing many properties of the binder both in solution and the electrode matrix and potentially causing undesired reactions. For example, even a brief exposure of Si particles to hydroxide can causing oxidation of Si particles and H_2 evolution [13,16,20,21]. A better understanding of the multiple roles played by the pre-lithiation of PAA binder in the electrode performance and fabrication would allow to find the optimum lamination condition as well as improved Si electrode.

In this study we quantify the effects of pre-lithiation treatment of PAA binder on the properties of such binder in solutions and slurries and characterize the performance of silicon-graphite (Si-Gr) composite electrodes fabricated using these binders. To reduce volume expansion in the electrode during electrochemical cycling, this composite electrode contained only ~15 wt% Si. For a fair comparison, the pre-lithiation of the binder, the fabrication and coating of the slurries, the thermal treatment of the laminate, and the testing protocols have been standardized.

2. Experimental section

2.1. Materials

PAA (M_n = 147 kDa, PDI = 4.9) and lithium hydroxide monohydrate were obtained from Sigma-Aldrich. Silicon nanoparticles (70–130 nm) were obtained from NanoAmor; graphite flakes (MagE, 2–4 μm) were obtained from Hitachi; conductive carbon particles (C45, 50–60 nm) were obtained from Timcal. The Si-Gr electrodes contained 73 wt% graphite, 15 wt% Si nanoparticles, 2 wt% conductive C and 10 wt% PAA binder. The active material loading was 2.6–3.0 mg cm^{-2} (see Table 1 for more detail) with a coating thickness between 20 and 25 μm. NCM523 cathodes contained 90 wt% $Li_{1.03}(Ni_{0.5}Co_{0.2}Mn_{0.3})_{0.97}O_2$, 5 wt% conductive carbon, and 5 wt% PVdF binder with a loading of 11.3 mg cm^{-2}. Copper (10 μm thick) and aluminum (20 μm thick) foils were used as current collectors for the anode and cathode, respectively. These electrodes were produced by the Cell Analysis, Modeling, and Prototyping (CAMP) facility of the Argonne National Laboratory. Before cell assembly, the electrodes were dried in a vacuum oven at 150 °C for 8 h. The specific capacities are reported per the total weight of the active materials; the discharge capacities are given unless stated otherwise.

Table 1
The loading density, initial specific capacity and coulombic efficiency, capacity retention and average capacity for half cells using Si-Gr electrodes fabricated with lithiated PAA binders.

Sam-ple	pH[a]	Loading density, mg cm^{-2}	Initial specific capacity,[b] mAh g^{-1}	Average capacity, mAh g^{-1}[c]	Initial Coulombic efficiency, %[d]	Capacity retention, %[e]
1	2.1	2.7	682	525	98.1	60
2	4.2	2.9	679	499	96.7	58
3	4.8	2.8	634	438	95.7	51
4	6.0	2.6	565	377	89.8	48
5	7.0	2.8	546	331	91.3	41
6	10.0	2.6	353	272	95.5	73
7	12.3	3.0	265	273	99.3	103

[a] From Table S1.
[b] Determined at the third formation cycle.
[c] Averaged capacity over 100 cycles.
[d] For the first cycle at a C/3 rate, after formation cycles at a C/20 rate.
[e] After 100 cycles at a C/3 rate.

Gen 2 electrolyte, which consists of 1.2 M $LiPF_6$ in a mixture of ethylene carbonate and ethyl methyl carbonate (3:7 w/w), was provided by Tomiyama Pure Chemical Industries. Fluoroethylene carbonate (FEC) used as the solid electrolyte interphase building additive was purchased from Solvay.

2.2. Preparation of pre-lithiated PAA solutions

PAA binders were weighed and dissolved in deionized water. After stirring the mixture overnight, calculated amount of LiOH and additional water were added to adjust the concentration of PAA to 10 wt%. The solutions were stirred for another 4 h, and the pH was determined using a Thermo Scientific Orion Star A215 m. The samples in Tables 1 and S1 are numbered in the order of the increased Li content (and pH).

2.3. Rheological measurements

Rheological characterization was carried out at 25 °C using a TA Instruments model Discovery HR-3 rheometer operating in a cone-plate geometry with a cone diameter of 20 mm and an angle of 2° (truncation 52 μm). To minimize water evaporation, a solvent trap cover was used. The apparent viscosity at different shear rates was measured in a flow ramp.

2.4. Peeling test

Peeling test of the Si-Gr composite electrode was conducted using an Instron 3343 universal tester. Laminates (25 mm × 75 mm) were attached to 3 M 600 Scotch adhesive tape. The electrode was peeled by pulling this tape at an angle of 180° and a constant displacement rate of

10 mm s^{-1}. The applied force was measured, and the load/displacement plots were obtained [22,23].

2.5. Cell assembly and electrochemical characterization

Cycling performance was evaluated using 2032-type stainless steel coin cells. The half cells were configured with a lithium metal electrode, a microporous polypropylene separator (Celgard 2325), a Si-Gr composite electrode, and 25 μL of Gen 2 electrolyte containing 10 wt% FEC. The cells were first subjected to three formation cycles at a C/20 rate followed by 100 cycles at a C/3 rate with the cell voltage maintained between 0.01 V and 1.5 V during this cycling. The current rate was derived from the actual capacity during the formation cycle. The electrochemical performance of each binder was determined by two parallel cells.

In full cells, the Si-Gr anode was paired with the NCM523 cathode. The cell testing protocol consisted of (i) three formation cycles at a C/20 rate, (ii) a hybrid pulse power characterization (HPPC) sequence to measure area specific impedance (AIS) at different depths of discharge (DOD), (iii) 92 aging cycles at a C/3 rate, (iv) another HPPC sequence, and (v) three final cycles at a C/20 rate to measure capacity fade. This gives a total of 100 cycles with the cell voltage maintained between 3.0 V and 4.2 V. In the HPPC test, the cells are charged at a C/3 rate to 4.2 V, discharged at C/3 rate to 10% DOD, and then rested at the open circuit voltage for 1 h. The hybrid pulse sequence includes a rectangular discharge pulse at a 3C rate applied for 10 s, a rest for 40 s, a charge pulse at a 2.25C rate applied for 10 s, and another rest for 60 s. The impedance was calculated by using the known current and the end-of-pulse voltage differences.

2.6. Post-cycling analysis

For the post-cycling characterization, the cells were disassembled in argon; the harvested electrodes were rinsed with anhydrous dimethyl carbonate and dried in a vacuum oven. The morphologies of the pristine and cycled electrodes were examined using a Hitachi S-4700-II scanning electron microscope (SEM). The energy dispersive X-ray (EDX) analysis was performed using a Bruker XFlash 6160 instrument. Fourier-transform infrared (FTIR) spectra of these electrodes were obtained using a Thermo Scientific Nicolet iS5 spectrometer.

3. Results and discussion

Pre-lithiated PAA samples were prepared by mixing the aqueous PAA solutions with LiOH as described above. Proticities and compositions of 10 wt% solutions are given in Table S1. Fig. 1a gives pH of these solutions as a function of the molar ratio *x*% of LiOH relative to the $-CO_2H$ groups calculated from the known stoichiometry. This pH dependence is reminiscent of the textbook strong base - weak acid titration curve. Below $x = 90\%$, the pH slowly increases from 2 to 6, which is followed by an abrupt change from 6 to 12, when *x* increases from 90% to 92%. As the Li^+ substitution progresses further, the pH increases from 12.0 to 12.6. The observed equivalence point of 92% is lower than expected from the stoichiometry, which we attribute to structural defects in the PAA polymer. In the following, the pre-lithiated PAA samples are denoted as PAA-pH and referred by pH of solutions in Fig. 1 that can be converted back to the lithiation ratio using Table S1.

Fig. 1b shows the apparent viscosity of pre-lithiated PAA solutions as a function of the shear rate (note the *logarithmic* scales in both axes). As seen from this plot, at low shear rates, the viscosities of PAA solutions dramatically increase as PAA becomes more lithiated. For instance, from pH 2.1 to pH 7.0, the viscosity at 1 s^{-1} increases nearly ten times from 1.1 to 10.7 Pa s. This significant increase can be attributed to the reduced mobility of the particles. As higher ionization of carboxylic groups in PAA can be expected at higher pH, their mobility would be much constrained, likely leading to much increased viscosity [24].

On the other hand, the shear thinning, which refers to the non-Newtonian behavior of fluids whose viscosity decreases under shear strain, was observed in all solutions. According to the power-law model,

$$\eta(\dot{\gamma}) = K(\dot{\gamma})^{n-1} \quad (1)$$

where η is the apparent viscosity, $\dot{\gamma}$ is the shear rate, *K* is the consistency index, and *n* is the flow index. The fluid is pseudoplastic (shear thinning) when $n < 1$, and a smaller *n* indicates stronger shear thinning. The parameters in eq. (1) were determined by fitting the apparent viscosity in the shear rate range of 10^2–10^3 s^{-1} (Table S2). It is seen that *n* decreases from ~0.83 at pH = 2.1 to ~0.40 at pH 12.3, indicating that a greater lithiation leads to a more pronounced shear thinning effect.

As we know, a higher viscosity of the continuous phase at a low shear rate can significantly improve the stability of aqueous suspensions by slowing down sedimentation and coalescence of suspended particles [25]. On the other hand, the shear thinning occurring at high shear rates makes it easier to mix slurries during their preparation, which is important for producing high quality laminates. Therefore, sufficiently high viscosity at low shear rates combined with sufficiently shear thinning (low viscosity at high shear rates) is a desired combination of properties for blending of Si nanoparticles in thick suspensions for a large scale lamination process.

It was observed at the Cell Analysis, Modeling, and Prototyping (CAMP) facility of Argonne National Laboratory that the **PAA-6.0** binder yields stable and uniform slurries, while **PAA-2.3** polymer yields poor-quality, coagulated slurries that result in uneven laminates. This behavior is partially rationalized by our results. Fig. 2 compares rheological properties of the slurries containing **PAA-6.0** and **PAA-2.1** binders (see the caption for the composition used). Compared to the binder solutions in Fig. 1, the viscosities of these slurries are much higher, but the same trends are observed. Compared to the **PAA-2.1** slurry, the **PAA-6.0** slurry has ten times higher viscosity at a low shear rate (better slurry stability during lamination), but the two viscosities

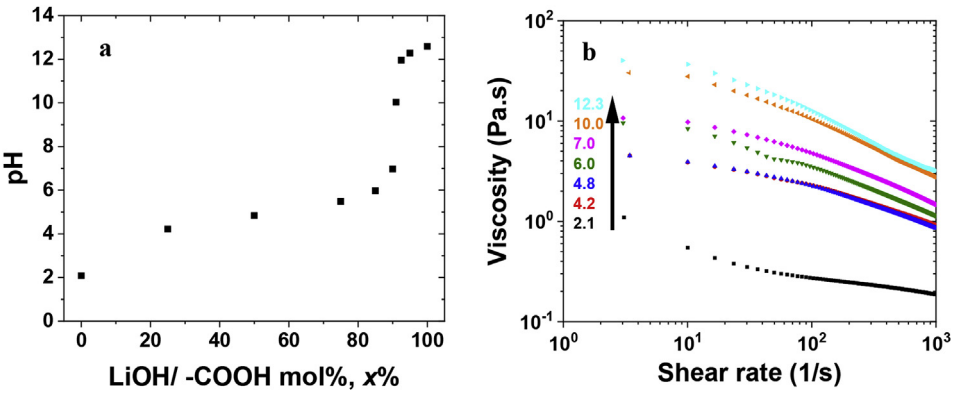

Fig. 1. A plot of pH *vs.* $LiOH/CO_2H$ mole ratio (a) and the apparent viscosity *vs.* the shear rate (b) for 10 wt% aqueous solutions of PAA. The pH of the solutions is color coded in panel b. Note the *logarithmic* scales in panel b. (For interpretation of the references to color in this figure legend, the reader is referred to the Web version of this article.)

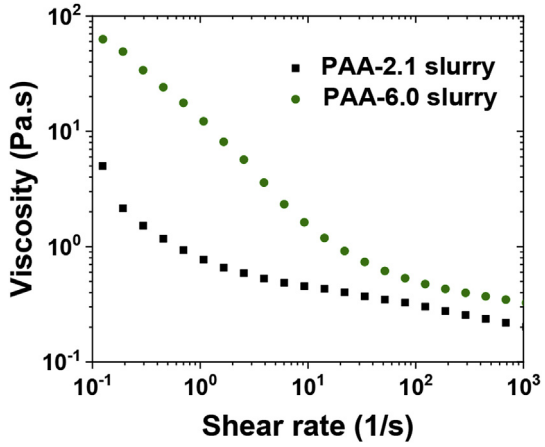

Fig. 2. A plot of the apparent viscosity *vs.* the shear rate (mind the logarithmic scales) for aqueous slurries containing 5 wt% PAA, 7.5 wt% Si, 36.5% graphite, and 1 wt% carbon particles. The pH of the aqueous solutions of the PAA binder is given in the plot.

become comparable at the shear rates exceeding 20 s^{-1} (these lower viscosities facilitate the mixing during preparation of the slurries). Thus, from the bulk processing point, the lithiated **PAA-6.0** binder does appear to have advantages over the untreated **PAA-2.1** binder.

To characterize the electrochemical performance, the binder solutions shown in Fig. 1 were used to fabricate Si-Gr composite electrodes as described in the experimental section, which were first evaluated in half cells (where these Si-Gr electrodes are paired with Li metal). Table 1 summarizes the cycling parameters, including the initial delithiation capacity, average capacity, and capacity retention. (Table 1 and Fig. 3). According to these tests, the cells using *less* lithiated PAA binders consistently demonstrated *better performance* in terms of their initial and average specific capacities and capacity retention after 100 cycles. For instance, during the formation cycles (Fig. 3a), **PAA-2.1** cell exhibited the highest initial specific capacity of 682 mAh g^{-1}. As pH increased to 7.0, the initial capacity decreased to 546 mAh g^{-1}. Strong capacity loss is seen in **PAA-10.0** and **PAA-12.3** cells. The observed capacities (353 mAh g^{-1} and 265 mAh g^{-1}) are similar to or lower than the specific capacity of graphite (372 mAh g^{-1}), suggesting that Si particles became consumed in reactions with LiOH (see the Introduction). The differential capacity profiles (Fig. 4 and Figure S1) confirm this conclusion. The characteristic peak of $Li_{15}Si_4$ at 0.43 V vs. Li/Li^+ is reduced as pH increases, and it disappears entirely at pH 12. Using voltage-capacity profiles, we estimate that the Si capacity decreased from 535 mAh g^{-1} for **PAA-2.1** electrode to 480 mAh/g for **PAA-7.0** electrode to 199 mAh g^{-1} for **PAA-10.0** electrode to just 19 mAh g^{-1} for **PAA-12.3** electrode. This dramatic loss of capacity indicates that Si particles become digested during fabrication of the electrode from basic solutions [13].

The Coulombic efficiency (CE) during the formation cycles shown in Fig. 3b shows some dependence of pH values. From pH 2.1 to 10, the CE of the second and third cycles generally decreases as a function of pH value of PAA. The pH 12.3 cell is an outlier with the exceptional high CE as well as the exceptionally low capacity. The low capacity of PAA-12.3 cell is due to the total loss of Si particles. Since the capacity is mainly from graphite, the higher CE is mainly due to more stable cycling of the graphite compared to Si. There is no clear trend for the first formation cycle, however, as this metric is related to the SEI formation. As at high pH the Si particles become more corroded, it is more than just the effect of the binder that affects the SEI formation process.

Following the formation cycles, all cells underwent 100 normal cycles at a C/3 rate. As shown in Fig. 3c, once again, the cells using less lithiated PAA binders (lower pH) exhibit better cycling performance and PAA-2.1 cell shows the best cycling performance. Figure S2 plots the initial capacity, average capacity (based on the 100 cycles) and capacity retention in different cells vs. the pH. Below pH ~ 7, the initial cell capacities slightly decrease with the increasing pH; this decrease (from 600 mAh g^{-1} to under 400 mAh g^{-1}) becomes more significant above pH 10, which is consistent with the loss of Si particles. The

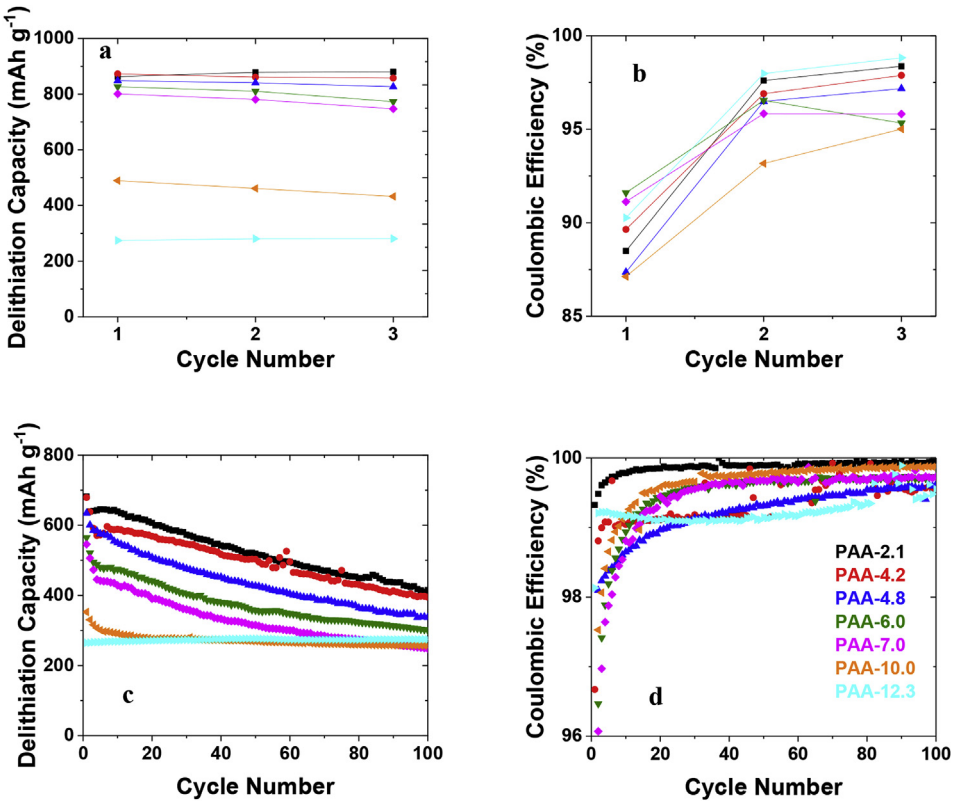

Fig. 3. Specific delithiation capacity (**a** and **c**) and coulombic efficiency profiles (**b** and **d**) of half cells assembled using lithiated PAA during formation cycles at a C/20 rate (**a** and **b**) and after 100 cycles at a C/3 rate (**c** and **d**). The pH of PAA solutions in Fig. 1 is color coded in panel d. (For interpretation of the references to color in this figure legend, the reader is referred to the Web version of this article.)

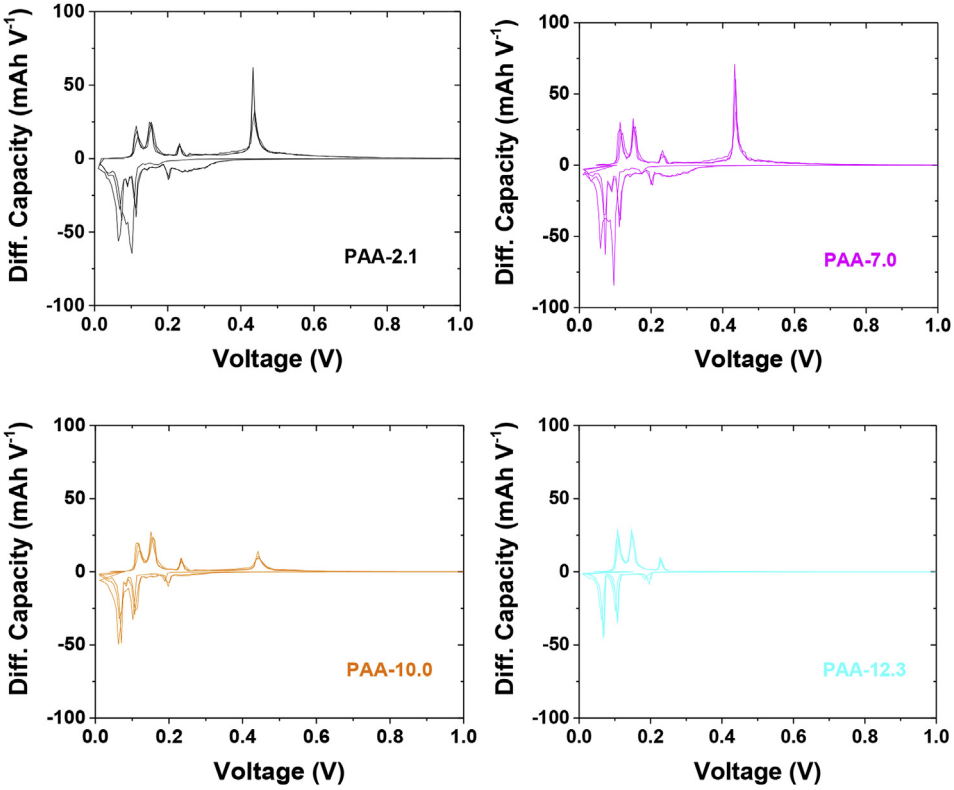

Fig. 4. Differential capacity (d*Q*/d*V*) for half cells containing Si-Gr composite electrodes using several PAA binders during the formation cycles at a C/20 rate. The pH of the PAA solutions in Fig. 1 is indicated in each panel.

average capacity also decreases at pH > 4, following the same trend as the initial capacity. From pH 4 to pH 7, the average capacity decreased by 36% from 500 mAh g^{-1} to ~320 mAh g^{-1}. Further increase in the pH led to a smaller decrease, and the average capacity stabilized at ~273 mAh g^{-1}.

Based on the cycling results, it is reasonable to expect that these trends could reflect the ability of the PAA binder to provide structural cohesion in the matrix, as it is a known concern for Si-Gr electrodes due to large volumetric changes in the Si particles during their lithiation and delithiation. In Fig. 5, a peeling test was used to assess the adhesive/cohesive strength of the electrode [26]. It shows a clear trend that average load/width values are higher for the binder with lower pH values (1.06 N cm^{-1} for PAA-2.1 compared to 0.64 N cm^{-1} for PAA-12.3). This test suggests that the increased lithiation of PAA *decreases* the cohesion in the matrix. This can be attributed to the reduced number of $-CO_2H$ groups that esterify siloxyl groups on the surface of Si particles, forming strong bonds between the polymer chains and the Si nanoparticles [27]. Clearly, the reduced cohesion also makes the PAA binder less efficient in countering the effects of volumetric changes of Si particles in the electrode matrix. We remind that according to previous report [28] pre-lithiated PAA is 40% less stiff than non-lithiated PAA, so the two trends (the cohesion and tensile strength) act in the same direction.

Surface characterization of the pristine and aged Si-Gr electrodes was conducted using the scanning electron microscopy (Fig. 6 and S3) and energy-dispersive X-ray spectroscopy (Figure S4 and Table S4). As shown in Fig. 6, pre-lithiation of PAA does not change the morphology of the pristine electrodes. However, there are notable differences in the oxygen content. For the **PAA-2.1** electrode, 2 at% O is present. As the lithiation progresses, the O content increased to 5–6 at% at pH 7.0 and 16 at% at pH 12.3, respectively, suggesting the increased Si oxidation due to partial digestion of Si nanoparticles by the hydroxide in solution. After 100 cycles, SEM images indicate multiple cracks for all electrodes excepting the pH 10 and 12.3 electrodes. As these cracks develop

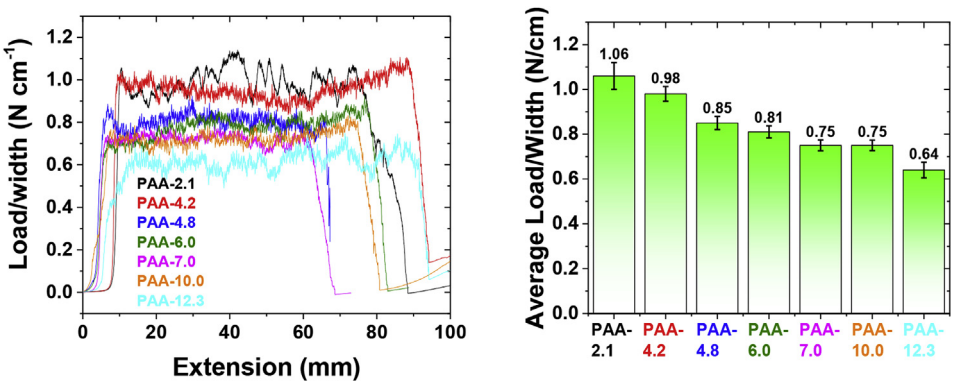

Fig. 5. The 180° peeling test for the Si-Gr electrode composed using different PAA binders (*left*). The load/width ratios averaged over a range of 50 mm for different electrodes (*right*). The pH of PAA solutions in Fig. 1 is indicated in the plots.

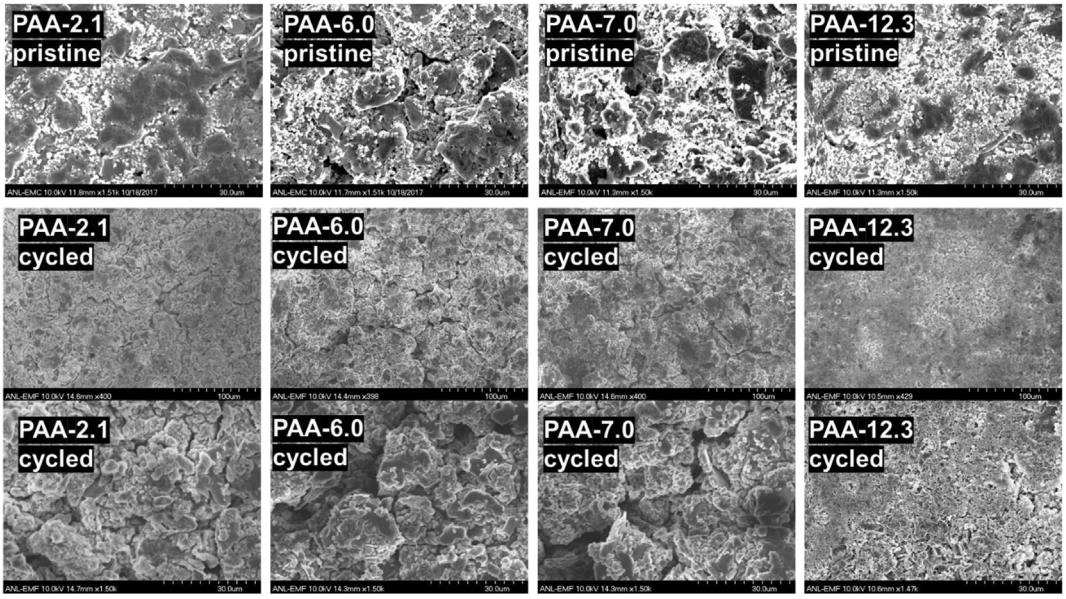

Fig. 6. SEM images of the Si-Gr composite electrodes harvested from the indicated cells before (*first row*, 1,500X magnification), and after (*second row*, 400X magnification), (*third row*, 1,500X magnification) 100 cycles at a C/3 rate. The pH of PAA solutions in Fig. 1 is indicated in the plots.

mainly in response to volumetric changes in Si particles, this observation suggests the depletion of Si particles in the latter two electrodes, which is in full agreement with our other results.

Fig. 7 shows the Fourier-transform infrared spectroscopy (FTIR) of the pristine and cycled electrodes. In the pristine electrodes, the intensities of the $-CO_2^-Li^+$ bands, which include the symmetric and antisymmetric stretching of the carboxylate groups at 1414 and 1562 cm^{-1}, respectively, and the CH_2 stretching of PAA at 1453 cm^{-1}, increase with the increasing pH, while the intensity of the C=O band from the $-CO_2H$ groups at 1685 cm^{-1} decreases, and the signal disappears entirely at pH $>$ 10. The broad peak at 900-1250 cm^{-1} which corresponds to the Si−O band increases in the amplitude in basic solutions, implying the growing oxidation of silicon due to its digestion by base. After cycling, all electrodes show the $-CO_2^-Li^+$ bands. The intensities of these bands decrease for pre-lithiated PAA samples with pH $>$ 7, suggesting gradual decomposition of these binders.

The cycling performance of the full cells, in which the Si-Gr electrode is paired with an NCM523 cathode, is shown in Fig. 8. The N/P ratio, initial and average capacities, the capacity retention, and the area specific impedance (ASI) are summarized in Table S5 and Figure S5. Low-pH cells still exhibited the superior performance, and **PAA-2.1** cell showed the best performance. As pH increased, the cycling performance generally deteriorated; the **PAA-6.0** cell demonstrated the second best performance. Compared to the half-cell results, the trend was not as clear possibly due to the cathode/anode matching issues (Table S5), yet we can confidently state that the pre-lithiation of PAA binder *did not improve* quantifiable metrics of the cycling performance.

4. Conclusion

In this study, we examine the effect of H^+/Li^+ exchange in the carboxylic groups of PAA binders (referred to as the pre-lithiation of PAA) on various properties of these polymers in solutions, slurries, and the electrodes; we also compared electrochemical cycling performance of Li-ion cells with Si-Gr composite electrodes containing these binders. Our study indicates that the pre-lithiation of PAA binder can indeed be beneficial from the technological standpoint; specifically, for slurry processing during fabrication of the electrode. At low shear rates, the pre-lithiation increases the viscosity of the aqueous slurries tenfold (so that they become less prone to sedimentation) while the viscosity at high shear rates ($>$ 20 s^{-1}) is not notably increased, so these slurries can be well stirred and homogenized during their preparation. These concerns are important on the industrial scale when processing time and slurry stability become important. However, from the standpoint of materials chemistry, the pre-lithiation of PAA binder can be detrimental, as it not only causes reduced adhesion/cohesion between the

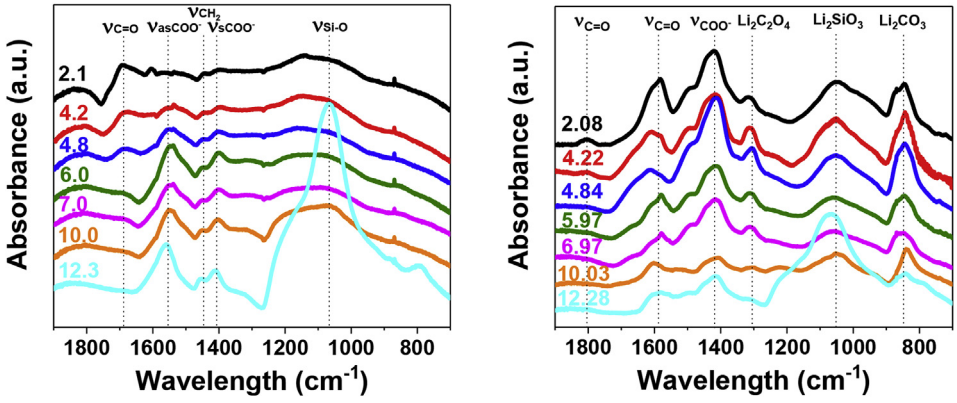

Fig. 7. FTIR of the Si-Gr electrodes before (*left*) and after (*right*) 100 cycles. The pH of PAA solutions in Fig. 1 is indicated in the plots. The vertical lines indicate the bands attributed at the top of the two panels.

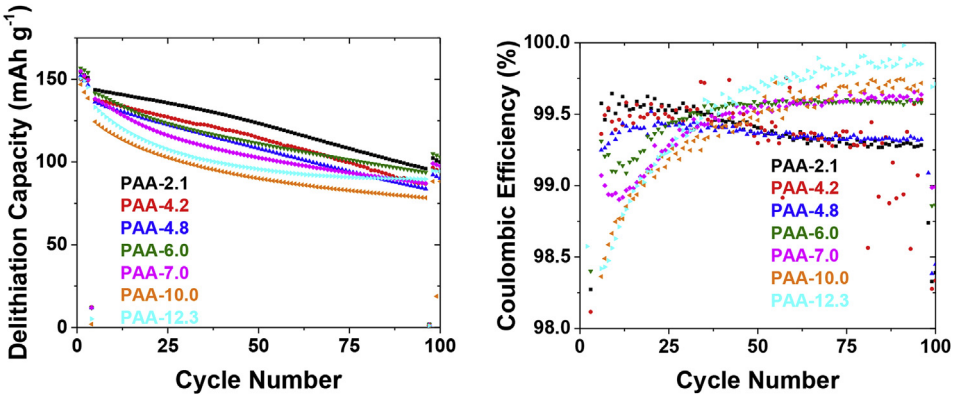

Fig. 8. Specific discharge capacity (*left*) and Columbic efficiency (*right*) for full cells. The pH of PAA solutions in Fig. 1 is indicated in the plot.

particles in the electrode matrix, as suggested by our peeling test, but also erodes the Si particles, evidenced by our post analysis results. As a result, the pre-lithiation of PAA binder can cause inferior cycling performance in both half and full cells. This detrimental behavior becomes more visible as pH increases over 7.

Thus, it appears that the current pre-lithiation treatments of PAA binder (favoring pH ~ 6–7) straddle the opposing trends in the cycling performance and rheological properties that benefit the large scale slurry preparation and electrode lamination process. To our knowledge, this is the first time that these two competing factors have been explicitly connected. We hope that this realization will lead to developing new binders or slurry formulas that do not require such an uneasy compromise.

Acknowledgments

This research is supported by the U. S. Department of Energy, Vehicle Technologies Office (DOE-VTO). Argonne National Laboratory is operated for DOE Office of Science by UChicago Argonne, LLC, under contract number DE-AC02-06CH11357. Use of the Center for Nanoscale Materials, an Office of Science user facility, was supported by the U.S. Department of Energy, Office of Science, Office of Basic Energy Sciences, under Contract No. DE-AC02-06CH11357. The authors would like to thank the Cell Analysis, Modeling, and Prototyping (CAMP) facility of Argonne National Laboratory for providing the electrode materials. The authors declare no competing financial interests.

Appendix A. Supplementary data

Supplementary data to this article can be found online at https://doi.org/10.1016/j.jpowsour.2019.01.068.

References

[1] R. Yazami, P. Touzain, A reversible graphite-lithium negative electrode for electrochemical generators, J. Power Sources 9 (3) (1983) 365–371.
[2] F.-H. Du, K.-X. Wang, J.-S. Chen, Strategies to succeed in improving the lithium-ion storage properties of silicon nanomaterials, J. Mater. Chem. 4 (1) (2016) 32–50.
[3] H. Wu, Y. Cui, Designing nanostructured Si anodes for high energy lithium ion batteries, Nano Today 7 (5) (2012) 414–429.
[4] L.Y. Beaulieu, K.W. Eberman, R.L. Turner, L.J. Krause, J.R. Dahn, Colossal reversible volume changes in lithium alloys, Electrochem. Solid State Lett. 4 (9) (2001) A137–A140.
[5] J.-Y. Li, Q. Xu, G. Li, Y.-X. Yin, L.-J. Wan, Y.-G. Guo, Research progress regarding Si-based anode materials towards practical application in high energy density Li-ion batteries, Mater. Chem. Front. 1 (9) (2017) 1691–1708.
[6] X.H. Liu, L. Zhong, S. Huang, S.X. Mao, T. Zhu, J.Y. Huang, Size-dependent fracture of silicon nanoparticles during lithiation, ACS Nano 6 (2) (2012) 1522–1531.
[7] C.K. Chan, R. Ruffo, S.S. Hong, Y. Cui, Surface chemistry and morphology of the solid electrolyte interphase on silicon nanowire lithium-ion battery anodes, J. Power Sources 189 (2) (2009) 1132–1140.
[8] T.-w. Kwon, J.W. Choi, A. Coskun, The emerging era of supramolecular polymeric binders in silicon anodes, Chem. Soc. Rev. 47 (6) (2018) 2145–2164.
[9] S. Choi, T.-w. Kwon, A. Coskun, J.W. Choi, Highly elastic binders integrating polyrotaxanes for silicon microparticle anodes in lithium ion batteries, Science 357 (6348) (2017) 279–283.
[10] I. Kovalenko, B. Zdyrko, A. Magasinski, B. Hertzberg, Z. Milicev, R. Burtovyy, I. Luzinov, G. Yushin, A major constituent of brown algae for use in high-capacity Li-ion batteries, Science 334 (6052) (2011) 75–79.
[11] N.S. Hochgatterer, M.R. Schweiger, S. Koller, P.R. Raimann, T. Wöhrle, C. Wurm, M. Winter, Silicon/graphite composite electrodes for high-capacity anodes: influence of binder chemistry on cycling stability, Electrochem. Solid State Lett. 11 (5) (2008) A76–A80.
[12] A. Magasinski, B. Zdyrko, I. Kovalenko, B. Hertzberg, R. Burtovyy, C.F. Huebner, T.F. Fuller, I. Luzinov, G. Yushin, Toward efficient binders for Li-ion battery Si-based anodes: polyacrylic acid, ACS Appl. Mater. Interfaces 2 (11) (2010) 3004–3010.
[13] C.C. Nguyen, T. Yoon, D.M. Seo, P. Guduru, B.L. Lucht, Systematic investigation of binders for silicon anodes: interactions of binder with silicon particles and electrolytes and effects of binders on solid electrolyte interphase formation, ACS Appl. Mater. Interfaces 8 (19) (2016) 12211–12220.
[14] S. Komaba, T. Ozeki, N. Yabuuchi, K. Shimomura, Polyacrylate as functional binder for silicon and graphite composite electrode in lithium-ion batteries, Electrochemistry 79 (1) (2011) 6–9.
[15] S. Jiang, B. Hu, R. Sahore, L. Zhang, H. Liu, L. Zhang, W. Lu, B. Zhao, Z. Zhang, Surface-functionalized silicon nanoparticles as anode material for lithium-ion battery, ACS Appl. Mater. Interfaces 10 (51) (2018) 44924–44931.
[16] L. Zhang, Y. Liu, B. Key, S.E. Trask, Z. Yang, W. Lu, Silicon nanoparticles: stability in aqueous slurries and the optimization of the oxide layer thickness for optimal electrochemical performance, ACS Appl. Mater. Interfaces 9 (38) (2017) 32727–32736.
[17] D. Dees, In Next Generation Anodes for Lithium-Ion Batteries: Overview, 2016 U.S. DOE Hydrogen and Fuel Cells Program and Vehicle Technologies Office Annual Merit Review and Peer Evaluation Meeting, Washington, D.C. , Washington, D.C. (2016).
[18] B. Hu, I.A. Shkrob, S. Zhang, L. Zhang, J. Zhang, Y. Li, C. Liao, Z. Zhang, W. Lu, L. Zhang, The existence of optimal molecular weight for poly(acrylic acid) binders in silicon/graphite composite anode for lithium-ion batteries, J. Power Sources 378 (2018) 671–676.
[19] S.E. Trask, K.Z. Pupek, J.A. Gilbert, M. Klett, B.J. Polzin, A.N. Jansen, D.P. Abraham, Performance of full cells containing carbonate-based LiFSI electrolytes and silicon-graphite negative electrodes, J. Electrochem. Soc. 163 (3) (2016) A345–A350.
[20] F. Erogbogbo, T. Lin, P.M. Tucciarone, K.M. LaJoie, L. Lai, G.D. Patki, P.N. Prasad, M.T. Swihart, On-demand hydrogen generation using nanosilicon: splitting water without light, heat, or electricity, Nano Lett. 13 (2) (2013) 451–456.
[21] A. Touidjine, M. Morcrette, M. Courty, C. Davoisne, M. Lejeune, N. Mariage, W. Porcher, D. Larcher, Partially oxidized silicon particles for stable Aqueous slurries and practical large-scale making of Si-based electrodes, J. Electrochem. Soc. 162 (8) (2015) A1466–A1475.
[22] M. Drdácký, J. Lesák, S. Rescic, Z. Slížková, P. Tiano, J. Valach, Standardization of peeling tests for assessing the cohesion and consolidation characteristics of historic stone surfaces, Mater. Struct. 45 (4) (2012) 505–520.
[23] P.-F. Cao, M. Naguib, Z. Du, E. Stacy, B. Li, T. Hong, K. Xing, D.N. Voylov, J. Li, D.L. Wood, A.P. Sokolov, J. Nanda, T. Saito, Effect of binder architecture on the performance of silicon/graphite composite anodes for lithium ion batteries, ACS Appl. Mater. Interfaces 10 (4) (2018) 3470–3478.
[24] Y. Chevalier, L. Belloni, J.B. Hayter, T. Zemb, Effect of interfacial charge on micellar structure, J. Phys. Fr. 46 (5) (1985) 749–759.
[25] S.G. Ward, R.L. Whitmore, Studies of the viscosity and sedimentation of suspensions Part 1. - the viscosity of suspension of spherical particles, Br. J. Appl. Phys. 1 (11) (1950) 286.
[26] B. Son, M.-H. Ryou, J. Choi, T. Lee, H.K. Yu, J.H. Kim, Y.M. Lee, Measurement and analysis of adhesion property of lithium-ion battery electrodes with SAICAS, ACS Appl. Mater. Interfaces 6 (1) (2014) 526–531.
[27] J.-S. Bridel, T. Azaïs, M. Morcrette, J.-M. Tarascon, D. Larcher, In situ observation and long-term reactivity of Si/C/CMC composites electrodes for Li-ion batteries, J. Electrochem. Soc. 158 (6) (2011) A750–A759.
[28] W. Porcher, S. Chazelle, A. Boulineau, N. Mariage, J.P. Alper, T. Van Rompaey, J.-S. Bridel, C. Haon, Understanding polyacrylic acid and lithium polyacrylate binder behavior in silicon based electrodes for Li-ion batteries, J. Electrochem. Soc. 164 (14) (2017) A3633–A3640.